A Low-Profile Wideband Circularly Polarized Metasurface Antenna Based on Characteristic Mode Theory

Shuangbing Liu[1,2], Lixia Yang[2], and Xianliang Wu[2]

[1]School of Electronic Engineering
Chaohu University, Hefei 238024, China

[2]School of Electronic Information Engineering
Anhui University, Hefei 230601, China
liushb@chu.edu.cn, lixiayang@yeah.net, xlwu@ahu.edu.cn

Abstract **–** A novel low-profile wideband circularly polarized metasurface (MTS) antenna is proposed. The characteristic mode analysis is used to investigate the operating mechanism of the MTS antenna. Then, the desired modes are chosen and excited by the annular ring slot combined with an L-shaped microstrip line. Simulation studies revealed that this type of feeding structure effectively excites the desired modes to accomplish wideband circular polarization and high-gain radiation. Experimental results show that the antenna has both the wide impedance bandwidth (IBW) and axial ratio bandwidth (ARBW), with a maximum radiation gain of 9.3 dBi and a −10 dB relative IBW and 3 dB relative ARBW of 39.8% and 30%, respectively.

Index Terms **–** characteristic mode analysis, circularly polarized slot antenna, metasurface, low-profile, wideband.

I. INTRODUCTION

Due to its advantages of generating and receiving at arbitrary polarization angles and anti-multipath interference, circularly polarized antennas are employed in wireless systems. Printed antennas are receiving considerable attention because of their compact size, low profile, simple design, uncomplicated design and fabrication, and low production cost [1]. However, these types of antennae suffer from narrow impedance bandwidth (IBW) and axial ratio bandwidth (ARBW). For example, Li et al. proposed a microstrip-fed slot antenna that stimulates circularly polarized radiation by loading capacitive or inductive loads in the annular slot, with 3 dB ARBWs of 5.5 percent and 6.7 %, respectively and radiation gain of 3 dBic [2]. The U-slot carved on the metal patch in the annular slot was used to obtain circular polarization in the annular-slot antenna [3]. The ARBW was 5.15% and the peak gain was 7.6 dBic. For L-shaped microstrip, a series feed approach was considered. Row developed a circularly polarized square ring slot antenna that was fed in series by an L-shaped microstrip and has shown a 3 dB ARBW of roughly 6% and a maximum radiation gain of 3.3 dBic [4]. A circularly polarized antenna with an ARBW of 8.9% and a maximum radiation gain of 6.5 dBic has been proposed in [5], which was fed by an annular ring slot with an L-shaped microstrip line.

Recently, metasurface (MTS) has been widely used in high-performance antennas, polarization modulation, and other applications. MTSs act as a reflector [6], polarization converters [7], or radiators [8–12]. The 3dB ARBW of the antenna increased to 23.4%, and the radiation gain of 7.0-7.6 dBic has been reported [8]. Cao et al. have developed a circularly polarized MTS antenna that was fed by an L-shaped slot and showed a 23.6% ARBW and a 7.3-8.1 dBic radiation gain [9]. Liu et al. reported a square array MTS antenna with four crossed slots for feeding [10]. The antenna showed a 14.5% ARBW and a 7 dBic radiation gain. In these antennas the MTS covers the dielectric layer of the feeding slot, resulting in a low profile and wide circularly polarized bandwidth, but insufficient radiation gain. An air layer [13] or a foam substrate [14] has been added between the MTS and the feeding structure of some antennas to improve the radiation gain. But this strategy has increased the antenna's profile as well as structural complexity.

II. STRUCTURE OF THE PROPOSED ANTENNA

The antenna structure and geometrical dimensions are shown in Fig. 1 and Table 1. The designed antenna consists of two layers of dielectric substrates. The relative dielectric constant of the upper layer is 3.5, with a thickness of h_2 = 2 mm. The MTS is formed by printing 5 × 5 square metal patch arrays on its upper surface, as shown in Fig. 1 (a). Each metal patch has dimensions of $p \times p$. The edge-to-edge width of the patches is g. The lower substrate has a relative dielectric constant of 4.4, with a thickness of h_1 = 0.8 mm, whose upper surface is a metal ground contact etched with an annular slot as

Submitted On: June 1, 2022
Accepted On: December 27, 2022
https://doi.org/10.13052/2022.ACES.J.371101

shown in Fig. 1 (b). The inner radius r_1 and outer radius r_2 of the annular ring slot are initially calculated by:

$$f \approx \frac{c}{\pi(r_1+r_2)\sqrt{\varepsilon_{eff}}}, \quad (1)$$

where f is the designed center operating frequency, c is the speed of light in free space and ε_{eff} is the effective relative permittivity considering the presence of different dielectric media on the two sides of the ring slot. A 50 Ω L-shaped microstrip feedline (width w_1) with a quarter-wavelength impedance transformer is designed on the bottom surface of the lower substrate as shown in Fig. 1 (c). The impedance transformer is a microstrip-line section of length l_2 and width w_2, which transforms the impedance seen at the outer slot boundary to the 50 Ω microstrip feedline.

To accomplish the low-profile characteristic, the ground contact is directly made with the two layers of dielectric substrates from the side as shown in Fig. 1 (d). Through the annular slot, the L-shaped microstrip feeder is couple-fed to the MTS in both x and y directions, with a phase difference of 90° between the two positions to produce circularly polarized radiation.

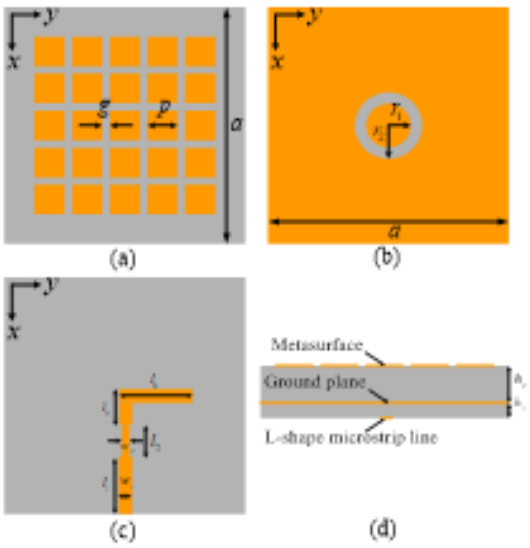

Fig. 1. Schematic diagram of the antenna structure. (a) MTS of 5 × 5 square patch arrays. (b) Ground contact with the annular slot. (c) L-shaped microstrip feed structure. (d) Side view of the antenna.

Table 1: Relevant parameters of wideband circularly polarized MTS antenna

Parameters	a	g	p	r_1	r_2	l_1
Unit (mm)	50	0.5	7.3	3.3	5.3	12.9
Parameters	l_2	l_3	l_4	w_1	w_2	
Unit (mm)	6.8	6.05	9.29	1.5	0.5	

III. WORKING MECHANISM OF CIRCULAR POLARIZATION

A. Characteristic mode analysis of the MTS

In recent years, characteristic mode analysis has been widely used in antenna design [16–19], which provides insight into the physical understanding of the antenna. The resonant frequency and potential contribution to the radiation of a mode are measured by the modal significance:

$$MS = \left| \frac{1}{1+j\lambda_n} \right|, \quad (2)$$

where λ_n are the eigenvalues. The range of MS is 0 to 1. If MS $\geq$ 0.707, the associated modes are significant. Otherwise, the associated modes are non-significant. When MS = 1, the mode resonates and radiates the most efficiently.

The modal properties of the MTS are explored to understand the functioning mechanism of circular polarization. The MTS with an infinite substrate and ground plate is simulated based on characteristic mode analysis. The MS of the four significant characteristic modes of the MTS is shown in Fig. 2. As can be seen, J_1 and J_2 are a pair of modes resonating at the same frequency of 7.2 GHz with the same MS. J_3 and J_4 exhibited the same resonant frequency, as well as a similar trend with frequency.

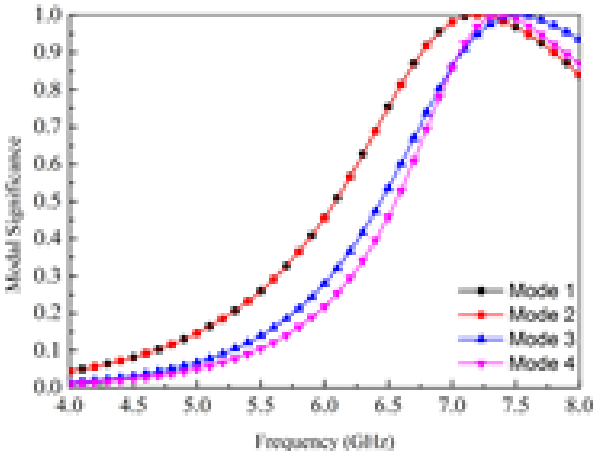

Fig. 2. MS of the four significant modes of the MTS.

Figure 3 shows the mode currents for the four modes at 7.2 GHz, with black arrows indicating the current direction. J_1 is in phase over the entire MTS and polarized in the y-direction. J_2 is identical to J_1, yet the polarization direction was rotated by 90° over the MTS plane. As a result of the symmetry of the MTS, J_1 and J_2 are a pair of orthogonal modes. As all of the currents are in phase, they both generate broadside radiation patterns, as shown in Figs. 4 (a) and (b). J_3 and J_4 were

self-symmetric in both the x and y directions. Due to the out-of-phase of the currents, a radiation null appears in the boresight, as shown in Figs. 4 (c) and (d). The modal radiation patterns are consistent with the results of modal current distributions. It can be concluded that J_1 and J_2 are the ideal unidirectional radiation modes, exciting either of which will form a linearly polarized antenna. Due to the orthogonality of the two modes themselves, the circularly polarized antenna will be formed in the scenario of simultaneous excitation of the two modes with a phase difference of 90°.

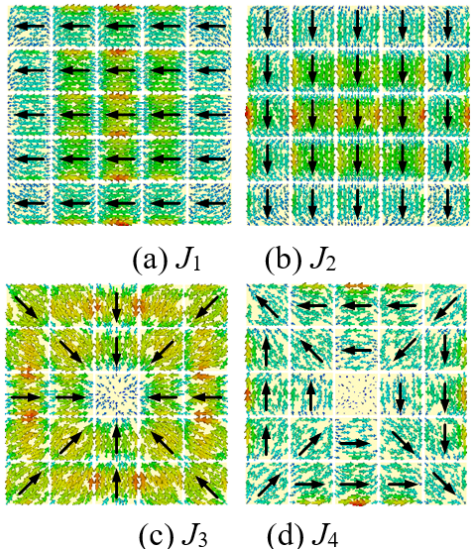

Fig. 3. Current distributions of the four characteristic modes at 7.2 GHz.

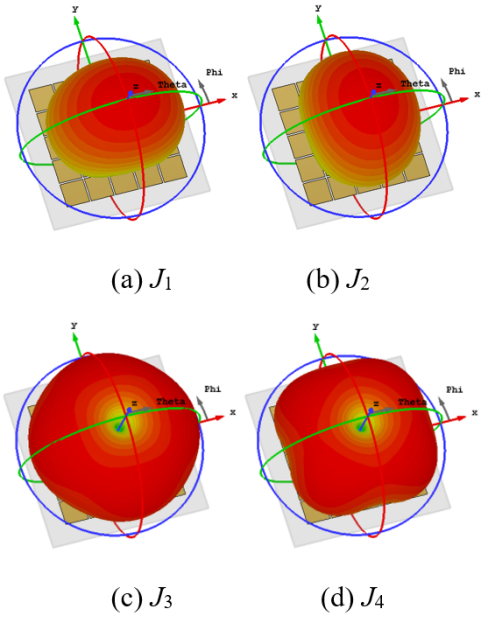

Fig. 4. Radiation patterns of the four characteristic modes at 7.2 GHz.

To acquire a circularly polarized broadside radiation pattern, the appropriate modes should be excited. Therefore, J_1 and J_2 are selected to generate the desired radiation pattern, while J_3 and J_4 are the unwanted modes.

B. Antenna feed network

The feeding structure is critical to exciting the desired mode. As shown in Fig. 3, it is easy to find that the maximum current distribution of J_1 and J_2 is at the center of the MTS, where the modes can be excited efficiently. But, the minimum current distribution of J_3 and J_4 is at the center of the MTS. The feeding structure should be positioned directly beneath the MTS's center patch. Furthermore, it is clear from Fig. 3 that the current densities of J_1 and J_2 on the middle patch are mostly dispersed near the patch's edge. Hence, the magnetic current coupled by feeding the annular-ring slot should be located where the maximum magnetic field of the desired mode J_1 and J_2 presents for maximum efficient coupling. In this way, the desired modes J_1 and J_2 can be most effectively excited by the feeding slot while the unwanted mode J_3 and J_4 will be suppressed. To obtain circularly polarized radiation, the feeding network has to excite both J_1 and J_2 at the same time and establish a 90° phase difference. Therefore, a single-feed network combining an annular-ring slot and an L-shaped microstrip line is adopted to excite the antenna, as shown in Figs. 1 (b) and (c).

Following this, simulations are performed on surface current distributions on the MTS at various phase excitations to explore the feed network's operating mechanism in greater depth. Figure 5 shows the surface current distributions on the MTS at two minimum frequencies of the antenna axial ratio (5.4 GHz and 6.7 GHz). The surface current is found to flow in the -x direction at 5.4 GHz with a phase angle of 0° and in the +y direction at a phase angle of 90°, as shown in Fig. 5 (a). As shown in Fig. 5 (b), the surface current is found to flow mainly in the +x direction at a frequency of 6.7 GHz and a phase angle of 0°, and in the –y direction at a phase angle of 90°. The results indicate that at each minimum of axial ratio, two orthogonal modes with a phase difference of 90° were excited, resulting in the acquisition of left-hand circularly polarized (LHCP) radiation in the broadside direction. Surprisingly, the distribution of surface currents flowing down the x-axis on the MTS's center patch is almost equal to that of J_2's characteristic mode current or is in an anti-phase state. Similarly, the distribution of surface currents flowing along the y-direction is nearly identical to that of the characteristic mode current or is in its anti-phase state. Maximum currents are predominantly centered on a few

patches at the center of the MTS at 5.4 GHz, but they are essentially spread over all patches over the MTS at 6.7 GHz, which may be found in the comparison of Figs. 5 (a) and (b). In other words, the axial ratio minimum at 5.4 GHz mainly resulted from the annular slot of the L-shaped microstrip feed, while that at 6.7 GHz is mainly attributed to the MTS.

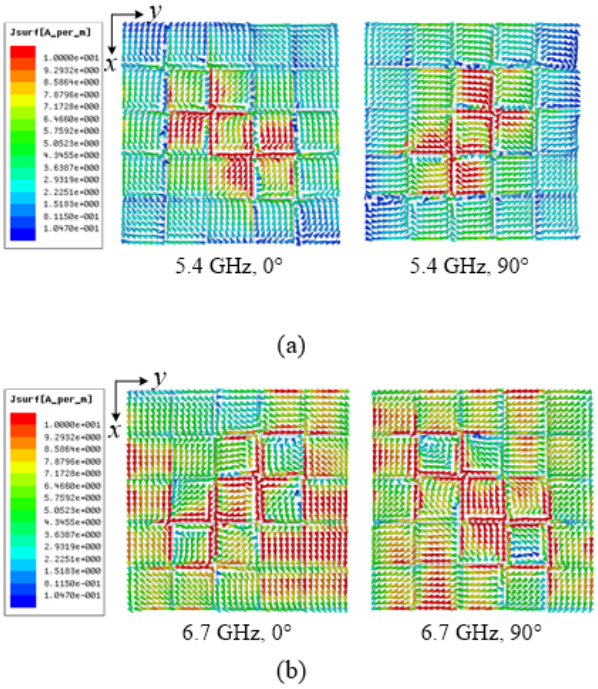

Fig. 5. Surface current distribution on the MTS at different excitation phases.

IV. PARAMETRIC STUDY

The parametric study is conducted to investigate the effects of key MTS parameters on the impedance bandwidth and ARBW of the broadband circularly polarized MTS antenna. The key parameters include the length of the square patch and the number of cells.

A. Effect of the length of the square patch (*p*)

Figure 6 shows the S_{11} and AR values of the circularly polarized MTS antenna for different lengths of the square patch. As shown in Fig. 6 (a), the variation in the length of the square patch has little effect on the reflection coefficient of the antenna. As the length increases, the impedance matching at the high frequencies deteriorates. It may be caused by the decrease of the resonant frequency of the characteristic modes J_1 and J_2 due to the increase of the length p. As shown in Fig. 6 (b), all lengths of the square patch yield two minimum points in their AR profiles. The frequencies of the two AR minimum points decrease with the increase of the length. AR is greater than 3 dB between 5.6–6.1 GHz for p = 8.1 mm. The optimal ARBW is obtained for p = 7.8 mm.

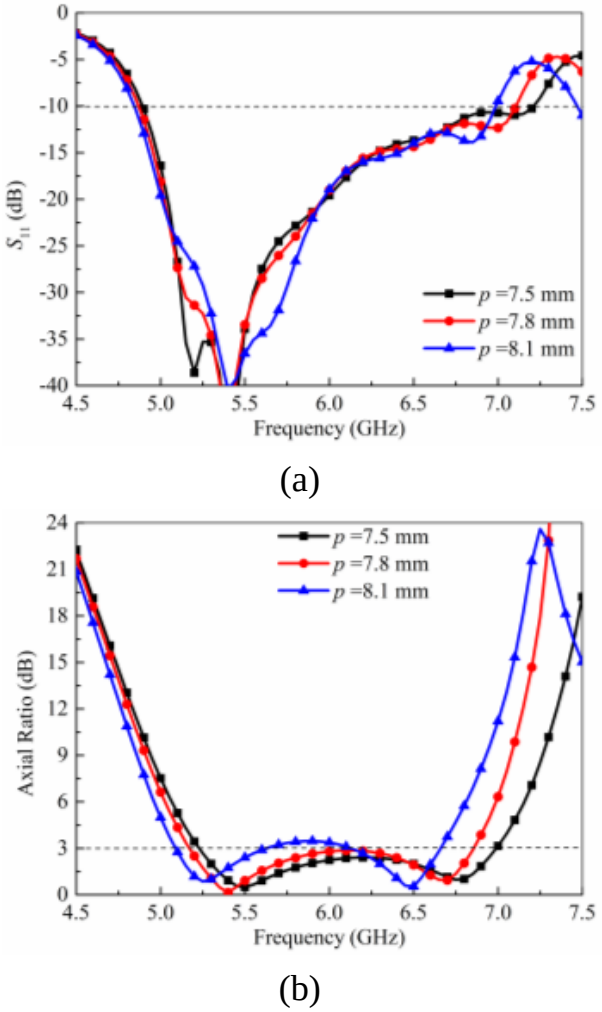

Fig. 6. Simulated (a) S_{11} and (b) AR values for different lengths of square patch.

B. Effect of the number of the cells

The S_{11} and AR values of the proposed MTS antenna are calculated for different cells of the MTS, including 3 × 3, 4 × 4, 5 × 5, and 6 × 6 cells, and are presented in Fig. 7. As shown in Fig. 7 (a), all configurations of the MTS antenna yield more than two resonant frequencies in their S_{11} profiles. Besides that, the number of MTS array elements has little influence on the IBW of the antenna, and the relative IBW of the antenna can be more than 30%. As shown in Fig. 7 (b), all configurations of the proposed antenna yield several minimum points in their AR profiles. One minimum point for 3 × 3 cells, two minimum points for 4 × 4 cells, and three minimum points for 6 × 6 cells. However, the 5 × 5 cell configuration yields an optimized result in terms of broad ARBW.

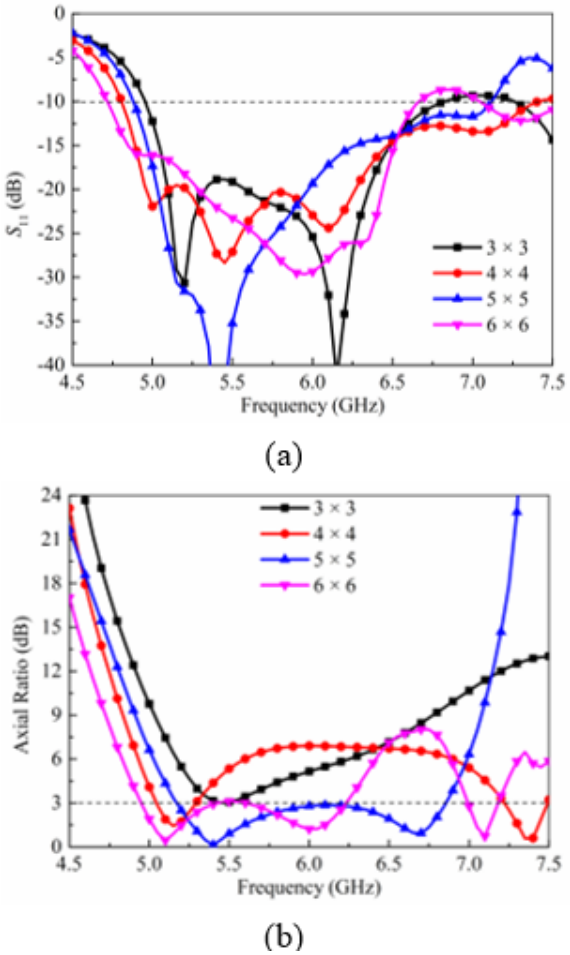

Fig. 7. Simulated (a) S_{11} and (b) AR values for different numbers of unit cells.

V. FABRICATION AND MEASUREMENT

The antenna is fabricated and measurements are performed to show the design effectiveness of the low profile wideband circularly polarized antenna. Figure 8 depicts the antenna's physical maps, with the front view on the left and the back view on the right. Agilent E5071C vector network analyzer is used to test the reflection coefficients of the antenna, and the results show −10 dB relative IBW of the antenna is 39.8% (4.82-7.22 GHz) as shown in Fig. 9. The test findings differ slightly from the simulation results, but they show a similar frequency variation trend. Furthermore, the operational bandwidths are essentially the same.

The antenna attains a 3 dB ARBW of 30% (5.1-6.9 GHz), which is slightly broader than the simulated results, as shown in Fig. 10. At 5.4 GHz and 6.7 GHz, the antenna axial ratios are 0.15 dB and 0.65 dB, respectively, indicating that circular polarization performed well. In the circularly polarized bandwidth, the gain

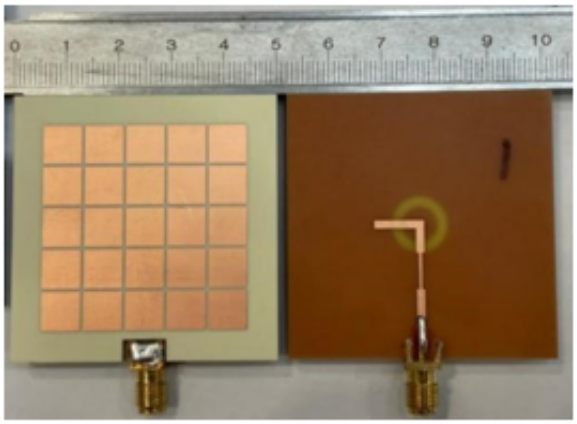

Fig. 8. Antenna physical map.

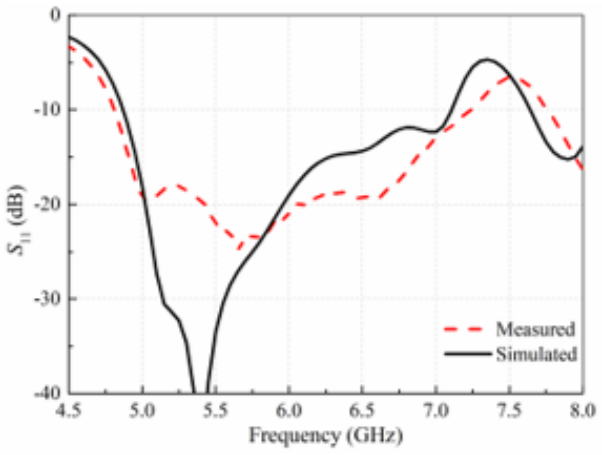

Fig. 9. Reflection coefficient of the antenna.

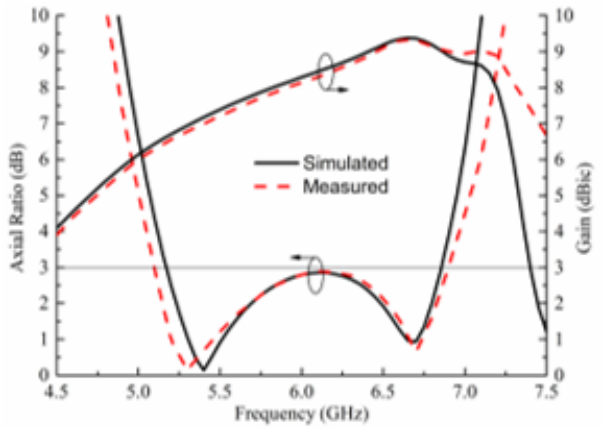

Fig. 10. Axial ratio and gain of the antenna.

in the boresight radiation direction of the antenna is higher than 6.3 dBic, and the peak gain reaches 9.3 dBic at 6.65 GHz, which means that the gain in the circularly polarized bandwidth is fluctuating within the range of 3 dB. As shown in Fig. 11, the simulated and the measured radiation efficiency are both higher than 88% throughout the 3 dB ARBW.

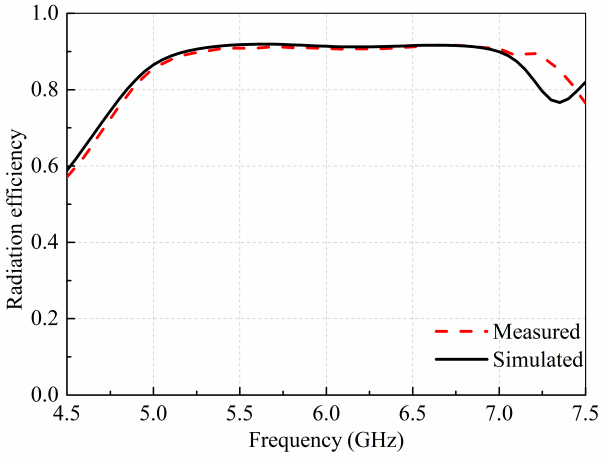

Fig. 11. Simulated and measured radiation efficiency.

Figure 12 shows the designed antenna's normalized far-field radiation pattern diagram, with (a) and (b) representing the radiation directly on the *xoz* and *yoz* planes at 5.4 GHz. Figures 12 (c) and (d) represent the radiation directly on the *xoz* and *yoz* planes at 6.7 GHz. The measured and predicted far-field radiation directional diagrams are almost identical, implying that the antenna produces steady and symmetric unidirectional axial radiation with clear LHCP radiation at both frequencies. The radiation gain is 7.0 dBic at 5.4 GHz, with a front-to-back ratio of 21.2 dB and a half-power beamwidth of 68°. The radiation gain is 9.3 dBic 6.7 GHz, with a front-to-back ratio of 24.8 dB and a half-power beamwidth of 46°. Additionally, the good symmetry in the radiation directional diagram suggests that the designed feed structure can effectively excite the J_1 and J_2 eigenmodes of the MTS in the characteristic mode analysis.

Performance comparisons between the designed antenna and the circularly polarized MTS antenna obtained from the literature are shown in Table 2. The developed antenna is found to have the widest 3 dB ARBW and higher radiation gain while preserving low-profile features. Overall, an antenna has been designed to have a low-profile, high gain, and wide bandwidth performance.

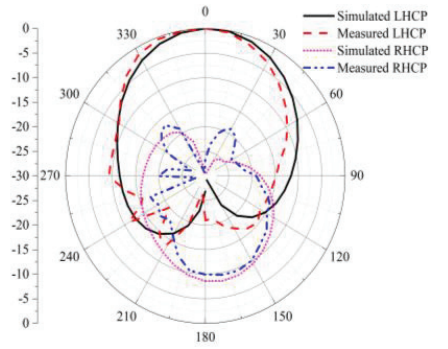

(a) Radiation pattern on *xoz* plane at 5.4 GHz

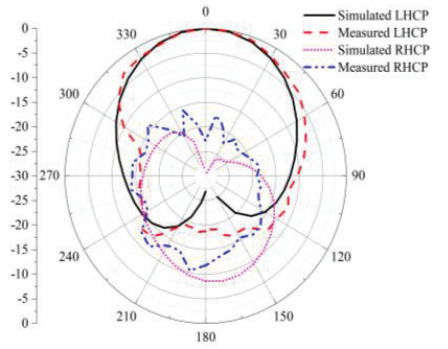

(b) Radiation pattern on *yoz* plane at 5.4 GHz

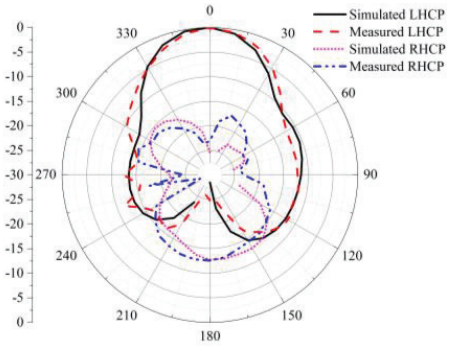

(c) Radiation pattern on *xoz* plane at 6.7 GHz

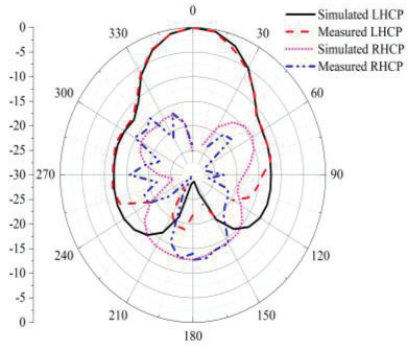

(d) Radiation pattern on *yoz* plane at 6.7 GHz

Fig. 12. Normalized far-field radiation pattern diagram of the designed antenna.

Table 2: Performance comparisons between the designed antenna and the antenna in the literature

Ref	Size (λ^3)	Frequency (GHz)	S_{11}	AR	Pink Gain (dBic)
[8]	0.58*0.58*0.0056	5.5	45.6%	23.4%	7.6
[9]	0.93*0.93*0.054	6.35	55.4%	23.6%	8.1
[10]	0.93*0.93*0.024	1.51	17.0%	14.5%	9.0
[11]	1.4*1.4*0.072	5.6	38.8%	14.3%	9.4
[12]	1.0*1.0*0.07	5.5	28.2%	20.9%	9.7
Proposed	1.0*1.0*0.056	6.0	39.8%	**30.0%**	9.3

VI. CONCLUSION

A wideband circularly polarized MTS antenna is proposed. The characteristic mode analysis is utilized to design the presented antenna. For the creation of circularly polarized radiation, a feed network consisting of an L-shaped microstrip and an annular slot etched on the ground contact is used to simultaneously excite the desired orthogonal modes and produce a phase difference of 90°. The experimental results and simulations show that the antenna has a low profile, high gain, and wide bandwidth, which is promising for modern wireless communication applications, such as satellites and radar, where high gain and wide bandwidth are crucial.

ACKNOWLEDGMENT

This work is supported by the Science Research Project of the Education Department of Anhui Province under Grant KJ2021A1024, the Domestic Visiting Study Program for Outstanding Young Talents in Colleges under Grant gxgnfx2021145.

REFERENCES

[1] A. J. A. Al-Gburi, Z. Zakaria, H. Alsariera, M. F. Akbar, I. M. Ibrahim, K. S. Ahmad, S. Ahmad, and S. S. Al-Bawri, "Broadband circular polarised printed antennas for indoor wireless communication systems: A comprehensive review," *Micromachines*, vol. 13, no. 7, pp. 1048, 2022.

[2] J. Li, C. Wang, A. Zhang, W. T. Joines, and Q. H. Liu, "Microstrip-line-fed reactively loaded circularly polarized annular-ring slot antenna," *J Electromagn Waves Appl.*, vol. 31, no. 1, pp. 101-110, 2017.

[3] N. Rasool, H. Kama, M. A. Basit, and M. Abdullah, "A low profile high gain ultra lightweight circularly polarized annular ring slot antenna for airborne and airship applications," *IEEE Access*, vol. 7, pp. 155048-155056, 2019.

[4] J. S. Row, "The design of a squarer-ring slot antenna for circular polarization," *IEEE Trans Antennas Propag*., vol. 53, no. 6, pp. 1967-1972, 2005.

[5] J. S. Row, "Design of aperture-coupled annular-ring microstrip antennas for circular polarization," *IEEE Trans Antennas Propag*., vol. 53, no. 5, pp. 1779-1784, 2005.

[6] H. Alwareth, I. M. Ibrahim, Z. Zakaria, A. J. A. Al-Gburi, S. Ahmed, and Z. A. Nasser, "A wideband high-gain microstrip array antenna integrated with frequency-selective surface for sub-6 GHz 5G applications," *Micromachines*, vol. 13, no. 8, pp. 1215, 2022.

[7] Z. J. Han, W. Song, and X. Q. Sheng, "Broadband circularly polarized antenna by using polarization conversion metasurface," *Applied Computational Electromagnetics Society (ACES) Journal*, vol. 35, no. 6, pp.656-661, 2020.

[8] S. X. Ta and I. Park, "Low-profile broadband circularly polarized patch antenna using metasurface," *IEEE Trans Antennas Propag*., vol. 63, no. 12, pp. 5929-5934, 2015.

[9] W. Q. Cao, B. N. Zhang B, W. Hong, and J. Jin, "L-shaped slot coupling-fed low-profile broadband circularly polarized patch antenna with metasurface," *J Electromagn Waves Appl.,* vol. 31, no. 1, pp. 111-120, 2017.

[10] S. Liu, D. Yang, and J. Pan, "A low-profile circularly polarized metasurface antenna with wide axial-ratio beamwidth," *IEEE Antennas Wirel Propag Lett*., vol. 18, no. 7, pp. 1438-1442, 2019.

[11] C. Zhao and C. F. Wang, "Characteristic mode design of wide band circularly polarized patch antenna consisting of H-shaped unit cells," *IEEE Access*, vol. 6, pp. 25292-25299, 2018.

[12] X. Gao, G. Tian, Z. Shou Z, and S. Li, "A low-profile broadband circularly polarized patch antenna based on characteristic mode analysis," *IEEE Antennas Wirel Propag Lett*., vol. 20, no. 2, pp. 214-218, 2021.

[13] A. Sharma, D. Gangwar, B. K. Kanaujia, and S. Dwari, "Gain enhancement and broadband RCS reduction of a circularly polarized aperture coupled annular-slot antenna using metasurface," *J Comput Electron*., vol. 17, no. 3, pp. 1037-1046, 2018.

[14] K. E. Kedze, H. Wang, and I. Park, "A metasurface-based wide-bandwidth and high-gain circularly polarized patch antenna," *IEEE Trans Antennas Propag*., vol. 70, no. 1, pp. 732-737, 2022.
[15] F. H. Lin and Z. N. Chen, "Low-profile wideband metasurface antennas using characteristic mode analysis," *IEEE Trans Antennas Propag*., vol. 65, no. 4, pp. 1706-1713, 2017.
[16] Z. Song, J. Zhu, L. Yang, P. Min, and F. H. Lin, "Wideband metasurface absorber (metabsorber) using characteristic mode analysis," *Opt Express*, vol. 29, no. 22, pp. 35387-35399, 2021.
[17] F. H. Lin and Z. N. Chen, "Resonant metasurface antennas with resonant apertures: Characteristic mode analysis and dual-polarized broadband low-profile design," *IEEE Trans Antennas Propag*., vol. 69, no. 6, pp. 3512-3516, 2021.
[18] B. B. Q. Elias, P. J. Soh, A. A. Al-Hadi, P. Akkaraekthalin, and G. A. Vandenbosch, "A review of antenna analysis using characteristic modes," *IEEE Access*, vol. 9, pp. 98833-98862, 2021.
[19] S. Z. Zhao, X. P. Li, Y. X. Chen, W. Y. Zhao, and Z. H. Qi, "A wide-beam metasurface antenna using pattern combination of characteristic modes," *Applied Computational Electromagnetics Society (ACES) Journal*, vol. 37, no. 1, pp. 41-49, 2022.

Shuangbing Liu was born in Anqing City, Anhui Province, China, in 1982. He received a B.S. degree in physics from Anhui Normal University, Wuhu, China, in 2005, and an M.S. degree in Electromagnetic and Microwave Technology from Anhui University, Hefei, China, in 2008.

Since 2017, he has been an Associate Professor at the Electronic Engineering Department, Chaohu University, Hefei, China. Now, he is a Visiting Scholar in Electronic Information Engineering Department, Anhui University, Hefei, China. His current research interest is antenna theory and design in wireless communication systems.

Lixia Yang was born in Enzhou, Hubei, China, in 1975. He received a B.S. degree in Physics from Hubei University, Wuhan, China, in 1997, and a Ph.D. degree in Radio Physics from Xidian University, Xi'an, China, in 2007. Since 2010, he has been an Associate Professor at the Communication Engineering Department, Jiangsu University, Zhenjiang, China. From 2010 to 2011, he was a Postdoctoral Research Fellow with the Electro-Science Laboratory (ESL), The Ohio State University, Columbus, OH, USA. From 2015 to 2016, he was a Visiting Scholar with the Institute of Space Science, The University of Texas at Dallas, Dallas, TX, USA. From 2016 to 2019, he has been a Professor and a Ph.D. supervisor, and the Chairman of the Communication Engineering Department, Jiangsu University. Since 2020, he has been a Distinguished Professor and a Ph.D. supervisor, and the Vice Dean of the School of Electronic and Information Engineering, Anhui University, Hefei, China. His research interests include wireless communication techniques, radio sciences, computational electromagnetics, and antenna theory and design in wireless communication systems. He is a member of the Editor Board of Radio Science Journal in China.

Xianliang Wu was born in Bozhou, Anhui, China, in 1955. He is a second-level Professor, a Ph.D. supervisor, and an Academic and Technological Leader of Anhui Province. He has been engaged in teaching and scientific research in electromagnetic field theory, mobile communications, electromagnetic scattering theory of complex targets, and electromagnetic field numerical calculation. He has presided over one key project and five normal projects of the National Natural Science Foundation of China, two doctoral fund projects of the Ministry of Education, one major national basic research project, one major national scientific and technological research project, and more than 20 provincial and ministerial level, enterprises and institutions commissioned development projects. He has authored or co-authored over 200 articles, including 185 articles indexed by SCI or EI. He has also authored two books. He is a Senior Member of the Chinese Institute of Electronics.